# The efficiency of ZnO / Platinum Octaethylporphyrin (PtOEP) Nanocomposite Photoanode at Dye-Sensitized Solar Cells

A.A. Abuelwafa[a,b*], M. S. H. Choudhury[c], M. Dongol[a], M. M. El-Nahass[d], T.Soga[b]

[a]Nano and Thin film lab. Physics Department, Faculty of Science, South Valley University, Qena 83523, Egypt.
[b]Department of Electrical and Mechanical Engineering, Nagoya Institute of Technology, Nagoya 466-8555, Japan.
[c]International Islamic University Chittagong, Chittagong-4203, Bangladesh
[d]Physics Department, Faculty of Education, Ain Shams University, Roxy, Cairo 11757, Egypt.

## Abstract:

In the present work, we have been studied the applications of ZnO /Platinum Octaethylporphyrin (PtOEP) Nanocomposites as Photoanodes for Dye-Sensitized Solar Cells (DSSC). The structural properties of ZnO:PtOEP Nanocomposites were examined by X-ray diffraction and Raman spectroscopy analysis which confirm the hexagonal wurtzite ZnO structure. Also, the simultaneous existence of PtOEP and ZnO in XRD and Raman mode was confirmed the formation of nanocomposite. Scanning Electron Microscopy (SEM) image of the surface morphology confirms the presence of PtOEP particle in the film. The variation in the weight ratios of ZnO:PtOEP is taken to optimize the performance of the DSSC. The photovoltaic and electrochemical impedance spectroscopy (EIS) data indicate that the optimum performance can be achieved at ZnO:PtOEP(1:0.009). Also, the (EIS) measurement for ZnO: PtOEP(1:0.009). photoanode shows displayed faster electron transport, significantly increased electron lifetime, and higher charge collection efficiency than those of pure ZnO.

---

**Key words:** PtOEP; Dye-sensitized solar cells (DSSC); hexagonal wurtzite; electrochemical impedance spectroscopy (EIS); electron lifetime

***Corresponding author***
***e-mail:*** ***Amr.abuelwafa@sci.svu.edu.eg*** (Amr Attia Abuelwafa )

## 1. Introduction

Dye-sensitized solar cells (DSSCs) or "Grätzel cell" have attracted significant research interest due to their low-cost production, simple manufacturing process, flexibility, transparency, and good performance under diffused light [1, 2, 3]. DSSCs become more, and more remarkable meanwhile an enormous variety of dyes (i.e. dye; e.g. N719, N3 [4], or organic dyes by monolayer adsorption or quantum dots (e.g. CdS, CdSe and PbS) and the also natural dyes [5]. Also, the photovoltaic performance of a DSSC essentially relies on the performance of the photoanode, which plays a fundamental role in the performance of DSSC due to its dye loading, electron transportation, and electron collection characteristics [6]. Wide bandgap semiconductors like $TiO_2$, ZnO, $Nb_2O_5$, and $SnO_2$ [7-9] nanoparticles were used as an efficient photoanode. Due to the small size of the nanoparticles, it can offer a large surface area and a comparatively high absorbency. Several researches have been proposed to control the charge recombination in the DSSC using doping of $TiO_2$ and ZnO with metal (Al, In, Bi, Cr, Ce, Mg, Au, Ag… etc.) [5, 6, 10, 11, 12]. Recently, new composite systems from hybrid materials of organic materials and metal oxide semiconductors in a nanometer scale have evolved as promising materials for DSSC. Due to the reduced probability of the recombination reaction by void the direct contact between metal oxide semiconductors and the redox electrolyte and reduced the recombination. Also, improved the charge separation and faster interfacial charge transfer than that of the pure metal oxide semiconductors [13, 14, 15, 16, 17, 18]. As examples on the these hybrid composite; polyaniline/ZnO [13], polypyrrole/ZnO [14],NiTPP/ZnO[15] PEDOTPSS/$TiO_2$[16], poly(N-vinylcarbazole)/$TiO_2$[17] andTiO2/polyisothianaphthene[18]. The porphyrin and its derivatives have been integrated into of DSSC in several ways. One of the most important advantages of using porphyrin and its derivatives are their redox properties, which aids for generating the porphyrin excited states that can be favorable as excellent dyes for dye DSSCs [19, 20, 21]. According to the best of our knowledge, the composite of ZnO/PtOEP as photoanode has been unexplored in DSSCs application. Therefore, the novel synthesis of ZnO/PtOEP is expected to have significant potential as photoanode in DSSCs.

## 2. Experimental techniques

### 2.1. Preparation of photoelectrode

PtOEP and ZnO nanoparticle were purchased from Aldrich and were used without further purification. ZnO/PtOEP photoanodes have been prepared by conventional blade coating method. The blade coating paste was consisting of 0.35 g ZnO nanoparticle (< 100 nm) and 2 ml ethanol (99.5%) along with various different weight ratios (as 1:0.00, 1:0.003, 1:0.006, 1:0.009, 1:0.012 and 1:0.015). The solution has been mixed vigorously using a homogenizer (Sonic VCX-130) at 60% amplitude, 1:3 pulse rates for 30 min. Before

coating, the prepared uniform paste was deposited on the pre-cleaned FTO substrates (~15 Ω/ square) using doctor blade method. The paste thus prepared was coated onto the FTO substrates using polyimide tape as frame and spacer. We coated the layer four times for obtaining a thick, adherent layer photoanode. All the samples were air dried at room temperature for one hour. The thickness of the film was 9~10 $\mu m$, measured by the surface profilometer (ULVAC alpha step-500). After coating, the films were dried at 100 ºC using a hot-plate for 10 min and compressed (Mini TEST Press-10) with 70 MPa compressions at 60 ºC for 1 min.

**2.2. Device fabrication**

The prepared photoanodes were immersed into an ethanol solution of the 0.5 mM N719 dye (Ruthenium-535 bis TBA, Solaronix). After 1 h the photoelectrodes were removed from the dye solution. The photoelectrodes were then immersed two or three times inside the methanol solution along with slight shaking to remove the extra loaded dye particles form the metal oxide nanoparticles. After cleaning by methanol, all the samples were dried by nitrogen flow. Finally, the DSC was fabricated by using a Pt-coated glass as a counter electrode, and by inserting a polymer film (Himilan, 50 µm) between the electrodes. The electrolyte (Iodolyte AN 50, Solaronix) was inserted into space between two electrodes by capillary action using a glass tube injector.

**2.3. Characterization**

Structural characterization was performed by XRD system (Rigaku RINT 2100 diffractometer) equipped with Cu target. The Ni-filtered Cu Kα radiation (λ=1.5408 Å) was used. The X-ray tube voltage and current were 40 kV and 30 mA, respectively. The Raman shift of the thin films was investigated by Raman Spectrometer (Jasco NRS-2100) at room temperature .with Ar and Kr laser lines operating at 514.5 nm it has a spectral resolution of 1 $cm^{-1}$. The morphology of ZnO:(PtOEP) Photoanodes was observed using a scanning electron microscopy (SEM, JSM-6510). The J/V characteristics of the devices were determined under white light illumination using standard solar irradiation of 100 $mW/cm^2$ (AM 1.5G) with a JASCO CEP-25BX spectrophotometer J/V measurement setup with a xenon lamp as the light source and a computer-controlled voltage-current source meter (Keithley 238) at 25 ºC. The impedance spectroscopy was measured at room temperature in the air with the frequency range of 0.02 to 1000 KHz using an impedance analyzer (Agilent 4284A) with a bias voltage of 0.6 V.

## 3. Results and discussions

### 3.1. Structural studies

#### 3.1.1. X-ray powder diffraction analysis

A typical XRD pattern of the pure ZnO and ZnO:PtOEP with different weight ratios are shown in **Fig 1**. All of the diffraction peaks, which correspond to the planes (100), (002), (101), and (102) are perfectly indexed to the hexagonal wurtzite ZnO structure (JCPDS 01-1136). The sharp and strong peaks indicate good crystallization of the samples. The diffraction peaks for PtOEP were visible for the lower and higher concentrations with a preferential orientation in the (001) direction [22, 23]. The peaks (001) and (002) related to PtOEP become more intense as the proportion of PtOEP increases in the composite. A small right shift has been observed for the positions of the all three diffraction peaks (100), (002), and (101) of wurtzite structured ZnO, while the percentage of PtOEP has been increased. It means that the spacing between the lattices planes corresponding to the peaks is changed [24]. Also, the increase of the intensities of the XRD peaks with increasing concentrations indicates an improvement in the crystalline quality of the synthesized samples. The crystallite sizes (*D*) have been estimated by applying the Scherrer formula [22]:

$$\mathrm{D} = \frac{K_S \lambda}{\beta \cos\theta} \qquad (1)$$

Where, $K_S$ = 0.94 is Scherrer`s constant, $\lambda$ is the X-ray wavelength of CuKα (0.15408 *nm*), $\theta$ is the Bragg's angle and $\beta$ is the Full Width at Half Maximum (FWMH) in radian. The results show that the average crystallite size increases from 33.7 to 48.3 nm with increasing percentages of PtOEP in the ZnO layer (**see Table 1**). X-ray profile analysis is generally used to estimate the average particle size. Particle size and lattice strain are the two major quantities responsible for change in peak broadening in an X-ray diffraction curve. Lattice strain is a measure of the distribution of lattice constants that arises from the crystal imperfections, such as lattice dislocations. The Williamson-Hall (W-H) analysis of diffraction peaks is used to estimate the crystallite size and lattice strain. Assuming that two terms (particle size and strain) contribute to peak broadening, are independent of each other and hence the observed peak breadth can be written as the sum of the particle size and strain as following equation((W-H) equation)[15]:

$$\beta_{hlk} \cos\theta = \frac{K\lambda}{D} + 4\varepsilon \sin\theta \qquad (2)$$

After fitting the data with a straight line to eqn. 2, the crystallite size and the strain $\varepsilon$ has been calculated from the intercept and slope of the linear fit respectively (figure not shown). The calculated particle sizes from the W-H plot are from 38.2 to 54.5 nm with increasing percentages of PtOEP in the ZnO layer (**see Table 1**). The crystallite size calculate from W-H analysis is slightly higher than that calculated from the Scherrer formula and this is because of the removal of strain contribution to the FWHM in the XRD peak

by W-H analysis. Hence, the resultant peak width is little lower than the same considered in the Scherrer formula. It is evident that the crystallite size increases and the lattice strain decreases with increasing PtOEP content. Grain boundaries, sinter stresses, stacking faults and coherency stress are the possible sources for development of strain in the ZnO host material. Moreover, the photoelectrode films were treated by hot-compression that can be the reason for some crystal disorder and in turn reductions in the lattice strain [15].

### 3.1.2. Raman study

**Fig. 2** displays the Raman spectra of pure ZnO and ZnO:PtOEP with different weight ratios at the range of 300-1000 $cm^{-1}$. These measurements confirmed the gradual increase of PtOEP content in the ZnO NPs. Two sharp Raman peaks at about 338 and 438 $cm^{-1}$ have been observed for ZnO film. Where the peak at 438 $cm^{-1}$ represents the $E_2^{high}$ vibration mode of wurtzite ZnO [25]. Also, all the samples show weak band around 438 $cm^{-1}$ is related to the vibration of Zn and O atoms in the hexagonal phase formation. On the other hand, the intensity of the peak at 438 $cm^{-1}$ decreased with increasing concentration which corroborated with the crystallinity behavior observed in XRD data. The presence of the $E_2^{high}$mode in all samples is the indication of the hexagonal ZnO structure, with the XRD results [26] and the 338 $cm^{-1}$ peak represents the $E_2^{high}$- $E_1^{low}$ vibration mode [26, 27]. For $E_2^{high}$ vibrational peak intensity has been reduced by increasing percentages of PtOEP in the ZnO samples. On the other hand, the $E_2^{high}$- $E_1^{low}$ peak intensity has been improved with the increasing percentages of PtOEP in the ZnO samples. Nevertheless, Raman vibration modes centered at 677, 721, 766,784 and 818 $cm^{-1}$ with different intensities belong to PtOEP respectively. The composite formation can be further confirmed by the simultaneous existence of PtOEP and ZnO Raman modes

### 3.2.3. Surface morphology

**Fig. 3** shows the surface morphology for (a) Pure ZnO, (b) ZnO/$PtOEP_{(0.009)}$, and (c) ZnO/$PtOEP_{(0.015)}$. In the pure ZnO, the surface looks smooth and homogeneous. While at ZnO/$PtOEP_{(0.009)}$, the surface morphology has not been changed a lot, only some black dots are visible, which represents some big PtOEP particles. By increasing the percentage of PtOEP in the sample, the PtOEP particles are found to create many big aggregates with different size and shapes with ZnO nanoparticles. This large-scale aggregation at high concentrations from PtOEP was a result of limited solubility of PtOEP in the ZnO blend.

### 3.2. Photovoltaic properties

Photovoltaic performance of the cells as an effect of weight ratios of ZnO:PtOEP is shown in **Fig. 4**. According to this figure the average device photovoltaic parameters such as open circuit voltage ($V_{OC}$), short-circuit current density ($J_{SC}$), fill factor (FF), and power conversion efficiency (PCE, η) for DSSC based on ZnO:PtOEP Photoanodes at different blend ratios are summarized in **Table2.** According to **Fig. 4** and

**Table 2,** the control device exhibited a PCE of 2.09% with $J_{sc}$ of 7.27 $mA/cm^2$ and *FF* of 0.52. Also, the optimum performance can be achieved at ZnO:$PtOEP_{(0.009)}$ ($J_{SC}$ of 8.05 $mA/cm^2$, FF of 0.57, and PCE of 2.58%), where the $J_{SC}$, and PCE enhanced about 23.44 and 10.72%, respectively compared to the control device. Thus, it is evident that the PtOEP concentration has an obvious effect on the photovoltaic performance. For the higher PtOEP concentration (ZnO:$PtOEP_{(0.012)}$and ZnO:$PtOEP_{(0.015)}$), the $J_{SC}$ value has been decreased to 7.11 and 6.84 $mA/cm^2$, also the PCE value has been reduced to 1.96 and 1.83%. Efficient operation of a DSSC device relies upon the minimization of possible recombination pathways occurring at the ZnO-dye-electrolyte interface, allowing efficient charge transport through the ZnO film, electrolyte, and subsequent charge collection at the device contacts. There are two possible recombination losses are to consider: i) the injected electrons may recombine either with oxidized dye molecules or ii) with the oxidized redox couple [15, 28, 29, 30, 31]. In order to reduce the recombination, at lower concentrations from PtOEP which is favorable for the effective electron transfer because the LUMO of PtOEP is little lower than the LUMO of N719 ( see **Fig. 5**), which is nearer to the conduction band of the metal oxide. Thus, it can be the reason for fast electron transfer at the dye-PtOEP/ZnO interface, and higher current density. Besides this, the inducing force in the electron transfer process inside the film might also be the reason for the improvement in the charge separation process as well as lowering the rates for the charge recombination. Without PtOEP the electrons transfer from dye to ZnO at a lower force, therefore there is a possibility of recombination for a couple of the electrons. However, for the higher concentration, the reason for decreasing the electron transfer can be described from the structural defects that have been created due to the formation of the considerable amount of bigger aggregates. These aggregates might be the reason for higher charge transport resistance at the metal oxide-dye to electrolyte interface which in turn reduces the $J_{SC}$. Another phenomenon is the generation of the singlet exciton to triplet exciton using the smaller amount from PtOEP incorporation and thus PtOEP particles inside the cells would lead to improving the exciton diffusion length, and solar cell performance [32, 33, 34]. Once the aggregation takes place at the higher concentrations from PtOEP in DSSCs, the power conversion efficiency dramatically decreases due to the localization of the triplet excitons in PtOEP phase islands resulting in lower *Jsc*, PCE, and $V_{OC}$ of the cells. Therefore, it gives lower $R_{SH}$ and high $R_S$ with a higher percentage of PtOEP. **Fig. 6** represents the EQE as a function of wavelength. High EQE signifies high optical absorption and hence a higher the incident photon-to-electron conversion efficiency [35]. According to **Fig. 6**, the range of wavelength of the incident light that contributes to photon to current conversion is varied from 350 to 750 nm. Ru-dye provides high quantum efficiency in the range of 500 to 550 nm [36, 37]. Therefore, the maximum conversion efficiency was found in this range. EQE curves follow the trends of short-circuit current density obtained from *J-V* curve measurements.

### 3.3. Impedance spectroscopy

The Electrochemical impedance spectroscopy (EIS) plays a vital role in understanding the interfacial kinetics and reactions of the fabricated DSSCs[20, 21, 38].The Nyquist plot with the standard equivalent circuit model (at inset) is shown in **Fig.7**. The fitting data is summarized in **Table 3**. *Rs* correspond to the overall series resistance of the device. The small semicircle at the high frequency is ascribed to the charge transfer process at the interfaces between the electrolyte and the Pt counter electrode, represented by $R_{CE}$. The larger semicircle at the lower frequency is related to the combination of i) transport process of the injected electrons within ZnO porous films and ii) the charge transfer process of the injected electrons at the interfaces between dye-loaded ZnO(ZnO/PtOEP) and the electrolyte, represented by $R_{AE}$. From **Table 3** we find that the values of $R_{S,}$ $R_{CE}$, and $R_{AE}$ were decreased by increasing the concentration of PtOEP and the lowest values for $R_S$, $R_{CE}$, and $R_{AE}$ have observed at ZnO:$PtOEP_{(0.009)}$. The lowest values of these resistances of the DSSC at ZnO:$PtOEP_{(0.009)}$ is consistent with the higher $J_{SC}$ and *FF* values of the cell, and with its higher performance Also, the decreasing in $R_{CE}$ with the increase of the concentration of PtOEP until ZnO:$PtOEP_{(0.009)}$ indicates faster charge migration across Pt-electrolyte interfaces and faster regeneration of the oxidized dye [39]. While the $R_S$, $R_{CE}$, and $R_{AE}$ values have been increased to 74.6, 217.4, and 116.2 Ω, respectively at ZnO:$PtOEP_{(0.015)}$ inside the cell. This may be due to the formation of PtOEP aggregates on the electrode surface, which might have caused a reduction in the surface area and a reduced dye uptake [40], resulting in a low value of current. This is evident from the SEM images shown in **Fig. 3 (c).**The bode phase plots for the samples are shown in **Fig. 8**. The characteristic time or electron lifetime $\tau_n$ in the DSSC based on PtOEP: ZnO nanoparticles is determined as the product of capacitance ($C_{AE}$) and electron transport resistance $R_{AE}$ at the ZnO/dye/electrolyte interface. From the Bode phase plot (**Fig. 8**) it is observed that the characteristic frequency peak (low-frequency region) shifts to lower frequency, as the concentration of PtOEP is increased until ZnO:$PtOEP_{(0.009)}$ after that shifts to the higher frequency at higher concentration from PtOEP. The characteristic frequency can be related to the inverse of electron lifetime [14, 41]. This indicates that the electron lifetime is higher at ZnO:$PtOEP_{(0.009)}$ and decreased at higher concentration. This result clearly explains the higher values of *Voc* and *FF* for DSSCs based on ZnO:$PtOEP_{(0.009)}$ Photoanodes compared to the control cell (0% PtOEP). The improvement in the electron lifetime was attributed to a reduced recombination between PtOEP: ZnO nanoparticles and the electrolyte. The high fill factor indicates the rapid diffusion of ions to the counter electrode as well as rapid transport of electrons through at ZnO:$PtOEP_{(0.009)}$ [40, 42].

## 4. Conclusions

The XRD pattern of the pure ZnO and ZnO: PtOEP has the diffraction peaks, which correspond to the planes (100), (002), (101) and (102), are perfectly indexed to the hexagonal wurtzite ZnO structure. Also, the XRD results show that the average crystallite size increases from 33.7 to 48.3 nm with increasing the concentrations of PtOEP. The weak peak at 438 $cm^{-1}$ in Raman spectra of ZnO and PtOEP:ZnO NP samples represents the $E_2^{high}$ vibration mode of wurtzite ZnO. The SEM image shows that higher level of PtOEP concentration creates the considerable number of micro-sized aggregates. This large-scale aggregation at high concentrations of PtOEP was a result of the limited solubility of PtOEP in the ZnO blend. The optimum performance can be achieved at $ZnO:PtOEP_{(0.009)}$ (JSC of 8.05 $mA/cm^2$, FF of 0.57, and PCE of 2.58%), where the JSC, and PCE enhanced about 23.44 and 10.72%, respectively. The smallest values of resistances for equivalent circuit model of impedance spectroscopy at of $ZnO:PtOEP_{(0.009)}$ based DSSC leads to upgrading in the photocurrent and solar cell performance. The electron lifetime is higher when the concentration of PtOEP is increased ($ZnO:PtOEP_{(0.009)}$) and decreased at higher concentrations of PtOEP. Thus, lower level of PtOEP can be a suitable choice for a low-cost efficient DSSC application.

# References.


[1] B. O'Regan, M. Grätzel, Nature **353**, 737 (1991).

[2] A. Suriani, M. Nurhafizah, A. Mohamed, M. Mamat, M. Malek, M. Ahmad, A. Pandikumar, N. Huang, Opt.-Int. J. LightElectron Opt. **139**, 291 (2017).

[3] P. Selvaraja, H. Baiga, T. K. Mallicka, J. Siviterb, A. Montecuccob, W. Lib, M. Paulb, T. Sweetc, M. Gaoc , A. R. Knoxb, S. Sundaram, Sol. Energy Mater. Sol. Cells **175,** 29 (2018).

[4]H.Nishikiori, Y.Uesugi, R.A.Setiawan, T. Fujii, W.Qian, M.A. El-Sayed, J. Phys. Chem. C 116, 4848(2012).

[5]O. Amiri, M. S.-Niasari, S. Bagheri, A. T. Yousefi, Sci. Rep. **6**, 25227 (2016).

[6] L. Vesce, R. Riccitelli, G. Soscia, T. M. Brown, A. Di Carlo, and A. Reale, J. Non-Crystalline Solid.356,(2010) 37–40.

[7]M. A. K. L. Dissanayake, J. M. K. W. Kumaria, G. K. R. Senadeeraa, C. A. Thotawatthagea, B.-E. Mellanderd, I. Albinssone, J. Photochem. Photobiology A: Chem. 349, 63 (2017) .

[8] M. Saito, S. Fujihara, Ene.Envir.Scien. 1,280 (2008).

[9] F. Lenzmann, J. Krueger, S. Burnside, K. Brooks, M. Grätzel, D. Gal, S. Rühle, D. Cahen, The Journal of Physical Chemistry B, **105**, 6347 (2001).

[10] M. Asemi, M. Ghanaatshoar, Appl. Phys. A 122,853 (2016).

[11] M. Asemi· A.Suddar, M. Ghanaatshoar, J Mater Sci: Mater Electron.28, 15233(2017).

[12] M. Asemi, M. Ghanaatshoar, J. Mater. Sci.52 (1), 489(2016).

[13] S. Zhu, W. Wei, X. Chen, M. Jiang, Z. Zhou, J. Solid State Chem. 190, 174 (2012).

[14] S. Chatterjee, A. Shit and A. K. Nandi, J. Mater. Chem. A 1,12302 (2013).

[15] M. S. H. Choudhury, S. Kato, N. Kishi, T. Soga, Jpn. J. Appl. Phys. 56,04CS05 (2017).

[16] C. S. Chou, C. S. Chou, Y. T. Kuo and C. P. Wang, Adv. Powder Technol. 24, 336 (2013).

[17]A. Ramar, R. Saraswathi, M. Rajkumar and S.-M. Chen, J. Phys. Chem. C 119, 23830 (2015).

[18] A. Ramar, R.Saraswathi, M. Rajkumar, S.-Ming Chen, J. Photochemistry and Photobiology A: Chemistry 329, 96 (2016).

[19] Ö. Birel, S. Nadeem, H. Duman, J Fluoresc.**27**,1075 (2017).

[20]N. V. Krishna, J. V. S .Krishna, S. P. Singh, L. Giribabu, L. Han, I. Bedja, R. K. Gupta, A. Islam,,J. Phys. Chem. C **121**,6464 (2017).

[21] T. Higashino, H. Imahori, Dalton Trans.44, 448 (2015).

[22] A. A. Abuelwafa, A. El-Denglawey, M. Dongol, M. M. El-Nahass, T. Soga, Optical Materials 49, 271 (2015).

[23]A. A. Abuelwafa, A. El-Denglawey, M. Dongol, M. M. El-Nahass, T. Soga, J. Alloy. Compd. **655**, 415 (2016).

[24] S.Kumar, M. Srivastava, J. Singh, S. Layek, M. Yashpal, A.Materny, A. K. Ojha, AIP Advances **5**,027109 (2015).

[25]B. Marí, F. J. Manjón, M. Mollar, J. Cembrero, R. Gómez, Appl, Surf. Sci. **252**, 2826 (2006).

[26]S. Akın, E. Erol, S. Sönmezoğlu, Electrochimica Acta **225**,243 (2017).

[27]R. K. Chava, M. Kang, J. Alloys Compd.692,67 ( 2017).

[28] E. Palomares, J. N. Clifford, S. A. Haque, T. Lutz, J. R. Durrant, Chem. Commun. **125**, 1464 (2002).

[29]H. J. Jo, J. E. Nam, D.-H. Kim, J. -K. Kang, J. Power Sources 249, 385 (2014).

[30] E. Kouhestanian, S.A.Mozaffari, M.Ranjbar, H. S. Amoli, M. H. Armanmehr, Super. Lattice. Micro **96**, 82 (2016).
[31]S.A. Mozaffari, M. Ranjbar, E. Kouhestanian, H. S. Amoli, M.H. Armanmeh, Mate.Sci. Semicond. Proces 40, 285 (2015).
[32]C. Lee, I. Hwang, C. C. Byeon, B. H. Kim, N. C. Greenham, Adv. Funct. Mater. **20**, 2945 (2010).
[33]K. Xiong, L. Hou, P. Wang, Y. Xia, D. Chen, B. Xiao, J. Lumine.**151**, 193 (2014).
[34]F. A. Angel, C. W. Tang, Organic Electronics **30**, 247 (2016).
[35]J. K. Tsai, W. D. Hsu, T. C. Wu, T. H. Meen, W. J. Chong, Nanoscale Res. Lett.**8**, 459 (2013).
[36]M. S. H. Choudhury, N. Kishi, T. Soga, J. Alloy. Compd. **656**, 476 (2016).
[37]R. Vittala, K.-C. Ho, Sustain. Energy. Rev.70, 920 (2017).
[38]A.Wei, Z.Zuo, J. Liu, K. Lin, Y.Zhao, J. Renewable Sustainable Energy 5 033101 (2013).
[39] C.-P. Lee, P.-W. Chen, C.-T. Li, Y.-J. Huang, S.-R. Li, L.-Y. Chang, P.-Y. Chen, L.-Y. Lin, R. Vittal, S.-S. Sun, J.-J. Lin, K.-C. Ho, J. Power Sources **325**, 209(2016).
[40]A. Mathew, G. M. Rao, N. Munichandraiah, Mate. Chem. Phys. **127**, 95 (2011).
[41]M. S. H. Choudhury, N. Kishi, T. Soga, Mater. Res. Bull. **80**, 135 (2016).
[42] A. A. Abuelwafa, M. Dongol, M. M. El-Nahass, T. Soga, Applied PhysicsA**124** 266 (2018).

## Figure caption

**Fig. 1**. The XRD patterns of ZnO and ZnO: PtOEP with different weight ratios photoelectrode films.

**Fig. 2.**Raman spectra of ZnO and ZnO: PtOEP with different weight ratios photoelectrode films.

**Fig. 3**. SEM image of a) Pure ZnO, (b) ZnO/$PtOEP_{(0.009)}$, and (c) ZnO/$PtOEP_{(0.015)}$.

**Fig. 4**. The J-V curve for the cells prepared by ZnO and ZnO: PtOEP with different weight ratios photoelectrode.

**Fig. 5**. The diagram of interfacial charge-transfer processes in DSSCs based on PtOEP:ZnO nanoparticles.

**Fig. 6**.EQE curve for the cells prepared by by ZnO and ZnO: PtOEP with different weight ratios photoelectrode.

**Fig. 7**. Nyquist plots of the of DSSC based on ZnO and ZnO: PtOEP with different weight ratios photoelectrode. The inset shows the basic RC model of the equivalent circuit.

**Fig. 8**.Bode phase plots of the of DSSC based on ZnO and ZnO: PtOEP with different weight ratios photoelectrode.

## Table caption

**Table. 1**. Structural parameters of PtOEP:ZnO nanocomposite.

**Table. 2**. Photovoltaic parameters of DSSC based on PtOEP: ZnO nanocomposite.

**Table.3**. Electrochemical impedance parameters of DSSC based on PtOEP:ZnO nanocomposite.

**FIG.1**

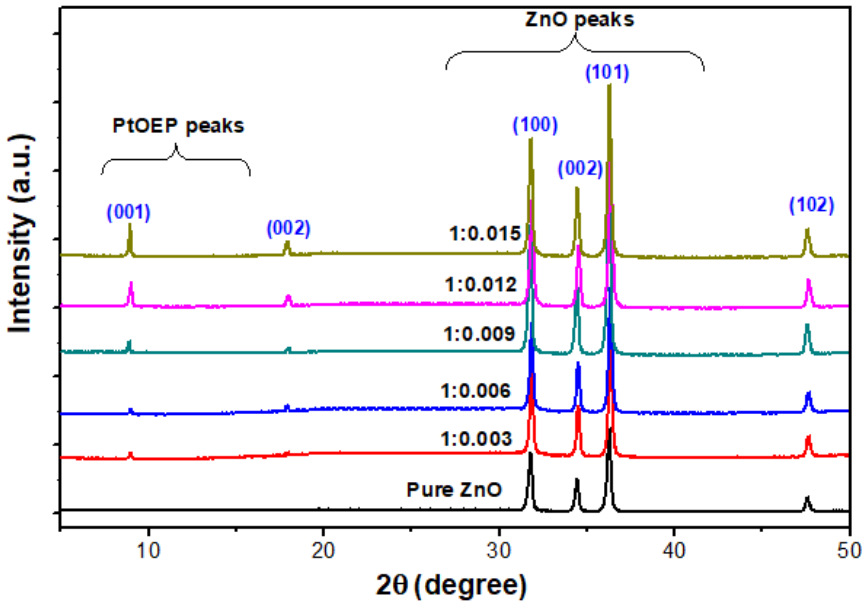
ZnO peaks
(101)
PtOEP peaks
(100)
(002)
(001)
(002)
(102)
1:0.015
1:0.012
1:0.009
1:0.006
1:0.003
Pure ZnO
Intensity (a.u.)
10
20
30
40
50
2θ (degree)

**FIG.2**

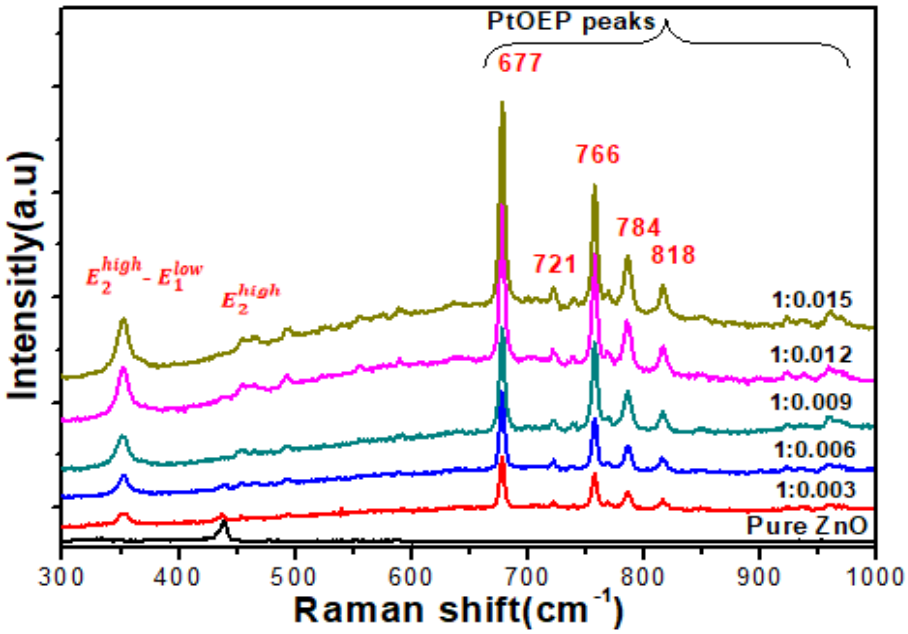
PtOEP peaks
677
766
784
818
721
$E_2^{high} - E_1^{low}$
$E_2^{high}$
1:0.015
1:0.012
1:0.009
1:0.006
1:0.003
Pure ZnO
Intensitly(a.u)
300
400
500
600
700
800
900
1000
Raman shift(cm$^{-1}$)

**FIG.3**

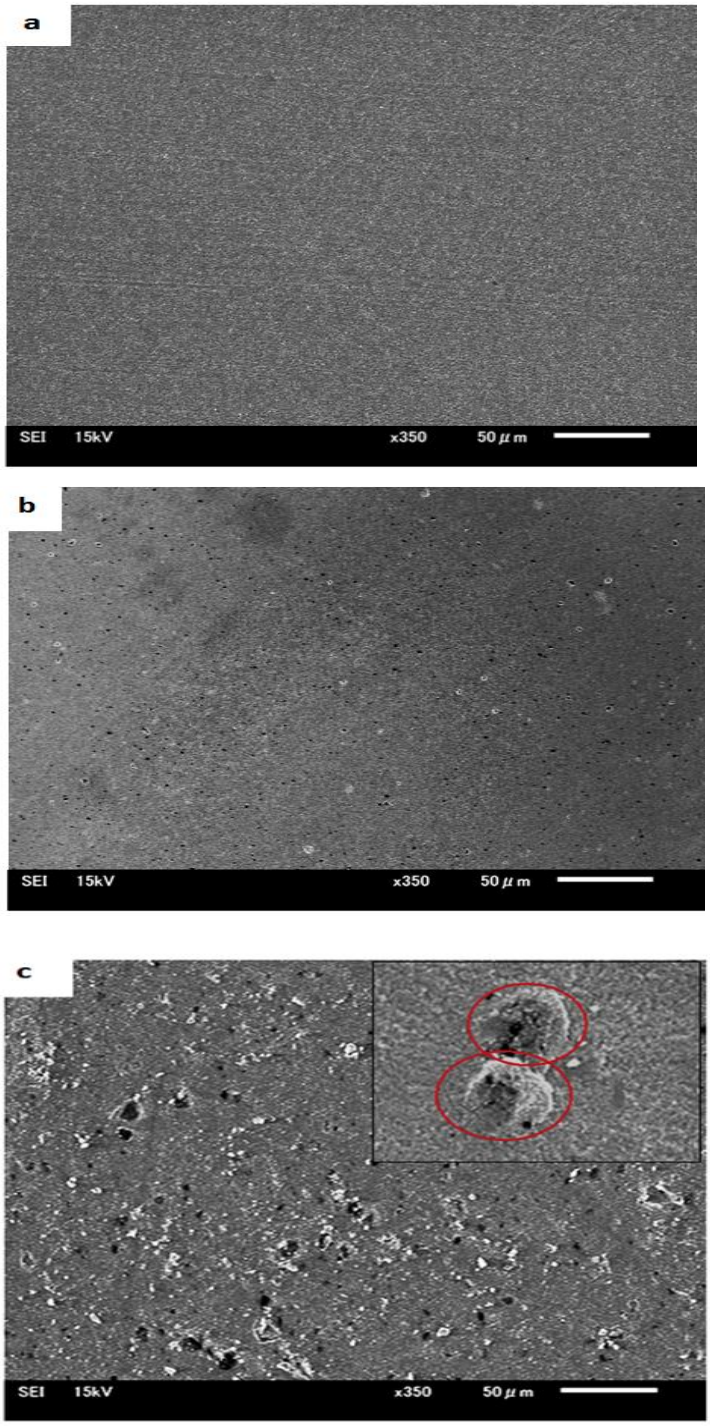

**FIG.4**

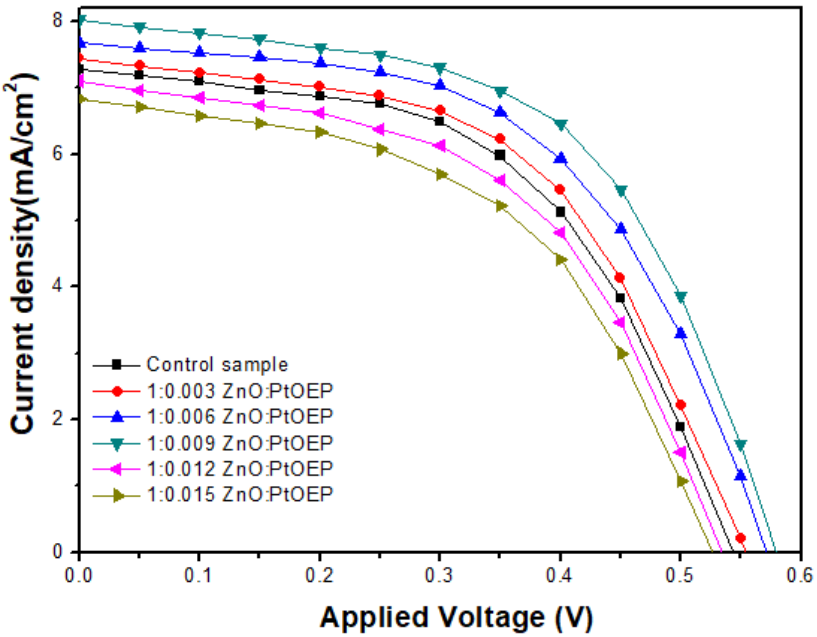
Current density(mA/cm$^2$)
Applied Voltage (V)
Control sample
1:0.003 ZnO:PtOEP
1:0.006 ZnO:PtOEP
1:0.009 ZnO:PtOEP
1:0.012 ZnO:PtOEP
1:0.015 ZnO:PtOEP
0
2
4
6
8
0.0
0.1
0.2
0.3
0.4
0.5
0.6

**FIG.5**

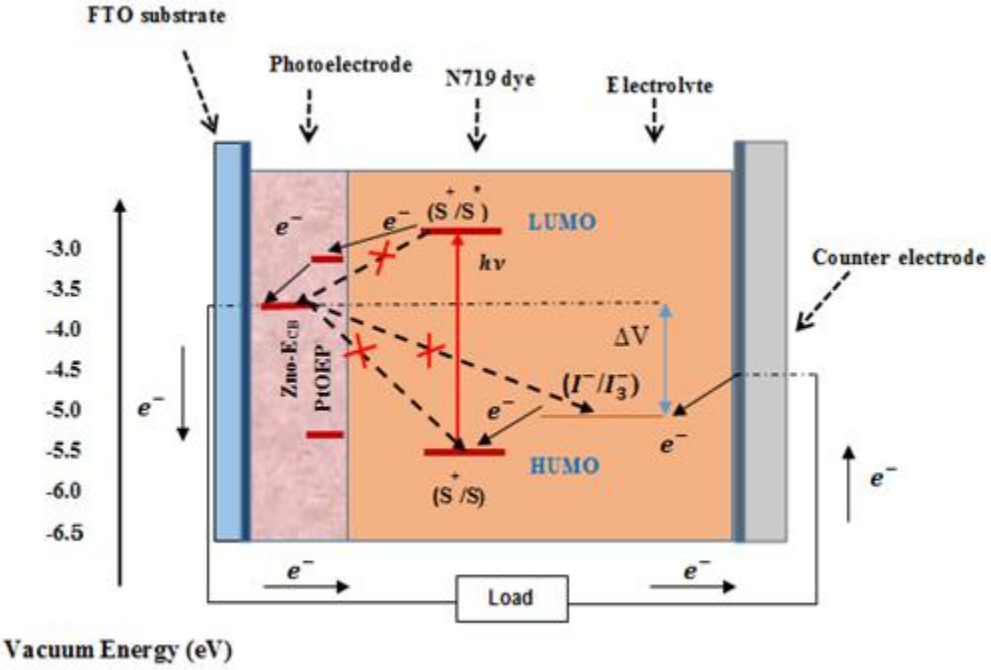
FTO substrate
Photoelectrode
N719 dye
Electrolyte
Counter electrode
LUMO
HUMO
hν
ΔV
Load
Vacuum Energy (eV)
-3.0
-3.5
-4.0
-4.5
-5.0
-5.5
-6.0
-6.5

FIG.6

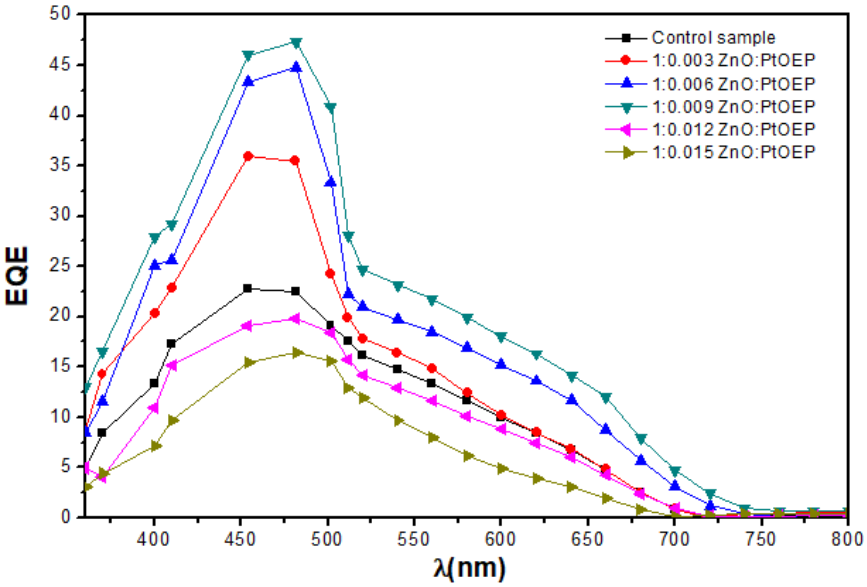
Control sample
1:0.003 ZnO:PtOEP
1:0.006 ZnO:PtOEP
1:0.009 ZnO:PtOEP
1:0.012 ZnO:PtOEP
1:0.015 ZnO:PtOEP
EQE
λ(nm)

FIG.7

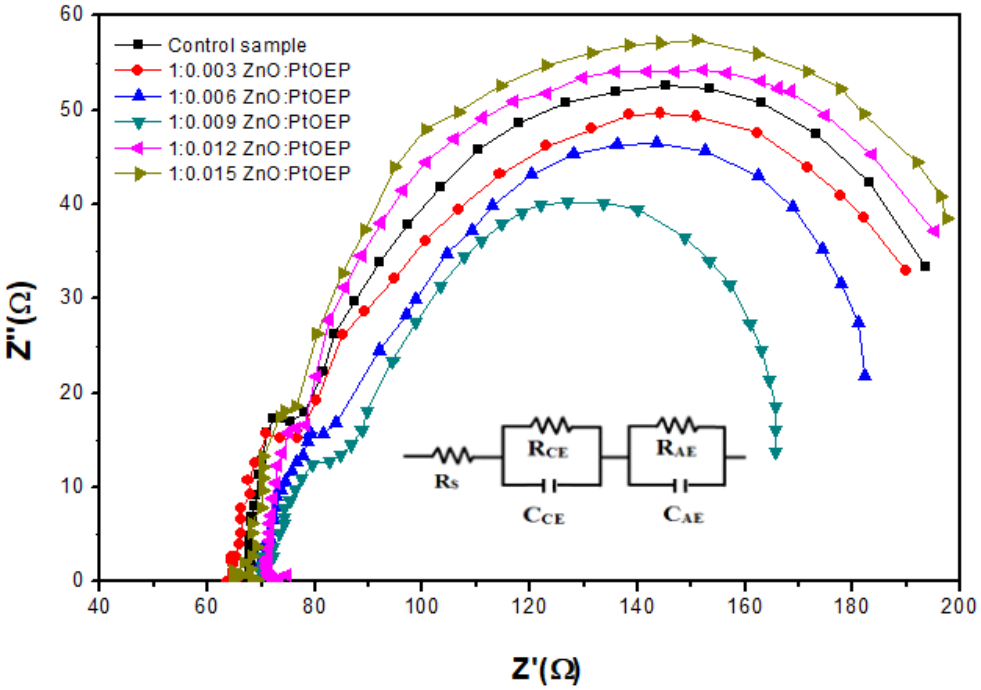
Control sample
1:0.003 ZnO:PtOEP
1:0.006 ZnO:PtOEP
1:0.009 ZnO:PtOEP
1:0.012 ZnO:PtOEP
1:0.015 ZnO:PtOEP
Z''(Ω)
Z'(Ω)
RS
RCE
RAE
CCE
CAE

**FIG.8**

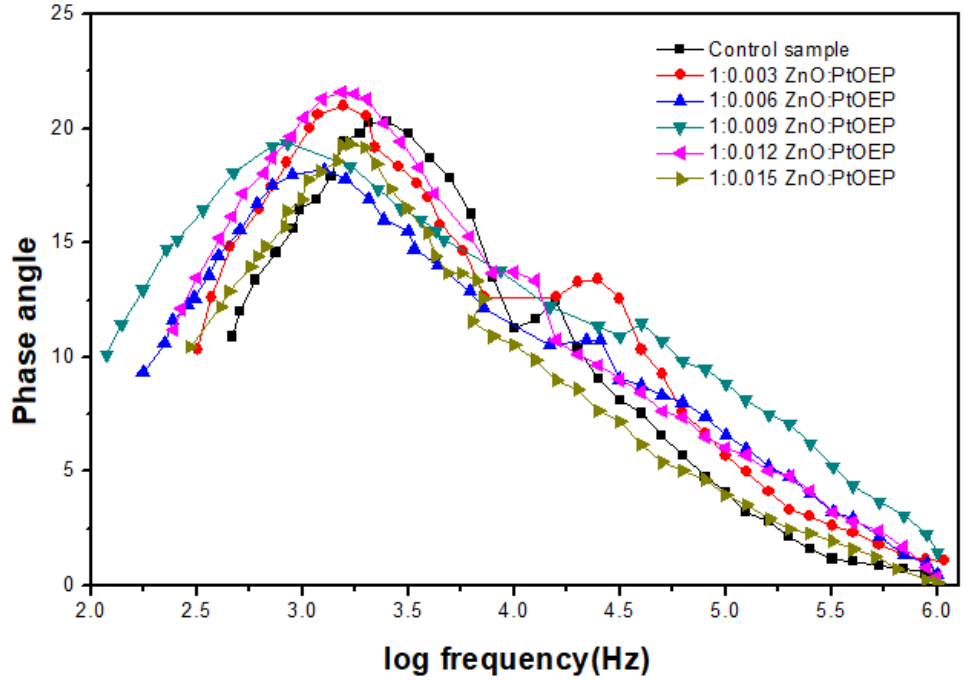
Control sample
1:0.003 ZnO:PtOEP
1:0.006 ZnO:PtOEP
1:0.009 ZnO:PtOEP
1:0.012 ZnO:PtOEP
1:0.015 ZnO:PtOEP
Phase angle
log frequency(Hz)

| photoelectrode | Crystallite size (nm) (Scherrer) | (W-H analysis) | |
|---|---|---|---|
| | | Particle size (nm) | Strain ($\varepsilon$) $\times 10^{-04}$ |
| **ZnO** | **33.78** | **38.23** | **9.32** |
| **1:0.003 ZnO:PtOEP** | **42.96** | **47.12** | **8.23** |
| **1:0.006 ZnO:PtOEP** | **45.54** | **49.46** | **7.75** |
| **1:0.009 ZnO:PtOEP** | **46.84** | **51.32** | **7.56** |
| **1:0.012 ZnO:PtOEP** | **46.98** | **52.45** | **7.47** |
| **1:0.015 ZnO:PtOEP** | **48.32** | **54.5** | **7.35** |

**Table.2**

| Cells | VOC(Volt) | Jsc(mA/cm$^2$) | FF% | η% |
|---|---|---|---|---|
| ZnO | 0.54 | 7.27 | 0.52 | 2.09 |
| 1:0.003 ZnO:PtOEP | 0.55 | 7.44 | 0.53 | 2.18 |
| 1:0.006 ZnO:PtOEP | 0.56 | 7.68 | 0.54 | 2.37 |
| 1:0.009 ZnO:PtOEP | 0.58 | 8.05 | 0.57 | 2.58 |
| 1:0.012 ZnO:PtOEP | 0.53 | 7.11 | 0.52 | 1.96 |
| 1:0.015 ZnO:PtOEP | 0.52 | 6.84 | 0.51 | 1.83 |

**Table.3**

| Cells | $R_S$(Ω) | $R_{CE}$(Ω) | $R_{AE}$(Ω) | $\tau_n$ (ms) |
|---|---|---|---|---|
| ZnO | 69.6 | 15.2 | 115.2 | 0.063 |
| 1:0.003 ZnO:PtOEP | 68.1 | 14.58 | 111.7 | 0.101 |
| 1:0.006 ZnO:PtOEP | 67.5 | 14.1 | 99.32 | 0.159 |
| 1:0.009 ZnO:PtOEP | 65.8 | 13 | 82.5 | 0.201 |
| 1:0.012 ZnO:PtOEP | 70.2 | 15.4 | 112.9 | 0.101 |
| 1:0.015 ZnO:PtOEP | 74.62 | 17.4 | 116.2 | 0.079 |

1

2